FLOW AND HEMOCOMPATIBILITY STUDY OF STRAIGHT-BLADED IMPELLER VADS

Victor Figueiredo Soares, Rodrigo Lima Stoeterau

Escola Politécnica da Universidade de São Paulo, São Paulo, Brasil.

ABSTRACT

Ventricular Assist Devices are continuous flow pumps that act as cardiac orthoses. The evaluation of the compatibility of such devices with blood involves, among other aspects, the study of thrombogenicity, hemolysis, and platelet activation. Computational Fluid Dynamics simulation is one of the tools used in this kind of evaluation. Thus, this work used Computational Fluid Dynamics simulations in the analysis of three Ventricular Assist Devices models under development, generating their velocity and pressure contours, their characteristic curves, and the distribution of shear stresses in their walls. A blood model has also been developed in order to estimate the damage inflicted on the blood by the devices. Steady-state simulations were performed, applying the Multiple Reference Frame method. The numerical blood modeling used the Lagrangean approach, with a discrete phase. The estimation of the damage on the blood was based on the relationship between the residence time of the discrete phase and the scalar shear stress. The prototype of one of the models was bench tested to validate the simulations. The simulation results relate the geometry of the models to the characteristics and magnitudes of the recirculation and stagnation regions and to the distribution of shear stresses. The energy performance of each pump and the blood damage index were used as comparison metrics between the devices.

Index Terms - ventricular assist device, CFD simulation, hemolysis, numerical blood model, multiple reference frame, discrete phase model.

1. INTRODUCTION

Cardiovascular diseases (CVDs) are one of the leading causes of death in the world, having claimed approximately 19 million lives in 2020, nearly 240 per 100,000 population. Eastern Europe and Central Asia presents the highest levels of mortality related to CVDs. Oceania, North and sub-Saharan Africa, the Middle East, Central Europe, and South and Southeast Asia also exhibit high mortality rates related to this group of diseases [1]. In Brazil, CVDs also occupy leading positions in the number of deaths, accounting for about 395,700 deaths in 2018 [2]. Among CVDs, heart failure, when in an advanced stage, may require a transplant or the adoption of a circulatory support system. In both cases a Ventricular Assist Device (VAD) may be necessary.

VADs are axial or centrifugal continuous flow pumps whose purpose is to assist the heart in pumping blood for patients with heart failure, and are used primarily as a bridge to transplant or in destination therapy [3, 4]. Its implant can be performed in the left ventricle (most common application, linked to the systemic circulation), right ventricle or biventricular implant [5].

In Brazil, heart transplants present important challenges, such as the long waiting list which can extend up to a year, and the regionalization of the hospital structure capable of performing this

kind of procedure [6, 7]. Although VADs make it possible to prolong the time a patient can stand in the transplant waiting list, the high cost of this therapy leads to resistance to its adoption by the Brazilian Unified Health System (SUS) [7]. Therefore, the development of technology that meets the Brazilian reality is an imperative.

Being an object alien to the human body, the implant of a VAD can be a source of issues associated with the circulatory system or infections. Stagnation zones or recirculating blood inside the device can act on the formation of thrombi (i.e., blood clots and fibrin). Exposing red blood cells (RBC) to high shear stress or to friction with VAD components can compromise their function or cause rupture of the cell membrane (hemolysis) [8, 9]. Regions prone to thrombi formation or with high shear stresses will be designated as critical zones.

Computational Fluid Dynamics (CFD) simulations are employed during the design phase in the identification of critical zones, allowing the optimization of models prior to prototyping.

Thus, this work proposes to analyze three models of centrifugal VADs under development at Escola Politécnica da USP through CFD simulation, in order to obtain the characteristic curves (rotational speed as a function of flow and pressure as a function of flow), the occurrence of recirculation zones, the distribution of shear stresses on the device walls and an estimation of hemolysis. Bench tests were performed with one of the models, confronting the performance results obtained in simulation with the experimental ones. The critical zones are studied through velocity and pressure contours and by velocity vectors, as well as by the shear stress distribution on the device walls. The hemolysis and platelet activation were estimated based on the model proposed by Giersiepen *et al.* [10] in conjunction with a modeling of the blood using a discrete phase.

2. MATERIALS AND METHODS

For each of the three models, CFD simulations were conducted using the software Ansys Fluent 22.1 (ANSYS, Inc.) adopting both water and a blood model as test fluid. The velocity and pressure contours, the performance through characteristic curves and the shear stresses were evaluated and the hemolysis promoted by the VADs were estimated.

A prototype of one of the models was made by additive manufacturing in resin to perform bench tests, which aim to obtain the model's characteristic curves and compare them with the results observed in the computational simulations. In these experiments, water was used as the test fluid.

2.1 Study object

The models under development are continuous-flow centrifugal pumps with straight-bladed open impeller. Figure 1 shows a sectional view of the VADs exposing the impeller of each model, where the drive systems are omitted. The geometrical aspects of each model are presented.

VAD-I1: its main dimensions are 53.40 mm in diameter and 65.25 mm in height with the motor. The inlet duct has a thread at its base that steers the flow in the direction of the impeller's rotation. The upper and lower housings are joined by an "L-shaped" socket.

VAD-DD1: its diameter is 42.0 mm and its height is 44.5 mm. Like the VAD-I1 model, the fit of the upper housing with the lower housing is an "L-shaped" socket.

VAD-R1/D1: the main dimensions of the model are 48.0 mm in diameter and 58.1 mm in height. The VAD-R1/D1 was designed for bench testing, where the pump actuation is external and the coupling between the actuator and the impeller is magnetic. The impeller is suspended

by contact bearings, with the upper bearing being associated with the inlet duct. The prototype model was obtained by additive manufacturing (SLA).
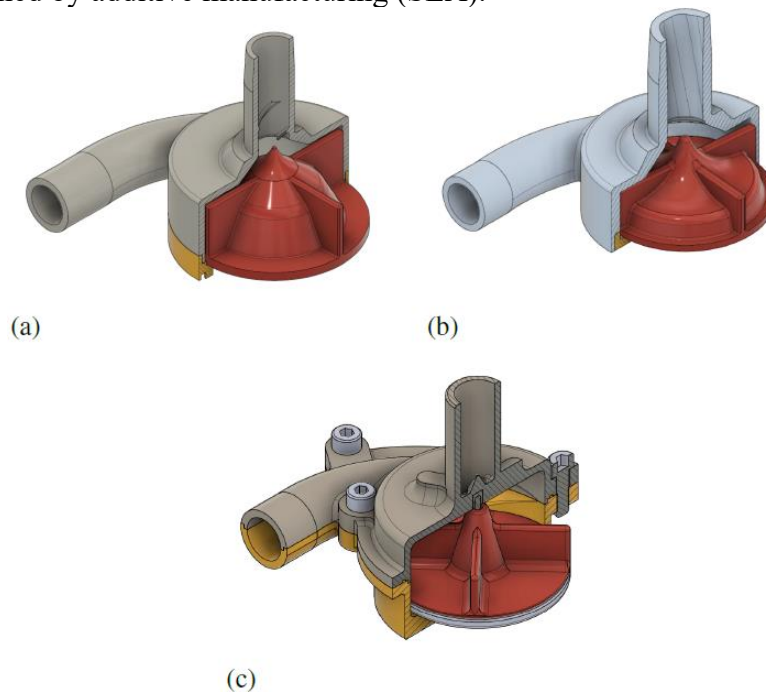

Figure 1: Sectional view of the (a) VAD-I1, (b) VAD-DD1 and (c) VAD-R1/D1 models. The motors and the impellers' magnetic coupling are omitted.

2.2 Thrombi and hemolysis

Thrombus formation in the context of VAD implant is associated, in summary, with stagnation or recirculation of blood, deposition of fibrin and denatured proteins in regions of the pump, and hemolysis [9]. Due to the complexity of the mechanisms responsible for thrombogenicity, it is difficult to develop a model to estimate it [11]. Some authors, such as Giersiepen *et al*. [10], Chiu *et al*. [12], and Bluestein *et al*. [13], use the platelet damage index as a method to estimate the thrombogenicity. However, the activation of platelets and the deposition of material (i.e., thrombus formation) do not necessarily occur in the same places [11]. The qualitative analysis of critical zones makes it possible to determine the location and magnitude of regions of stagnation, recirculation, or high shear stresses and to evaluate sites where thrombus formation will occur [14].

Hemolysis is defined as the rupture of the RBC's cell membrane, so its contents (such as hemoglobin) leak into the plasma. It occurs when the cells are submitted to high shear stresses, by pressure variations or by contact with surfaces subject to relative movement, where the exposure time to these factors is relevant [4, 15]. These stresses are influenced by the design and manufacturing of the device, highlighting the gap between the impeller and the housing, impeller speed, bearing type, and surface roughness [9].

Among the mechanisms that promote damage to RBCs, shear stress is the most important. Such damage is not only linked to the release of hemoglobin into the plasma, but also to morphological changes that reduce the cell's lifespan [15].

2.3 Blood rheology and physiological requirements

Blood is a suspension of cells in a fluid composed of 90% water, so its density varies around 1050 kg/m³. Although blood is a non-Newtonian fluid, in studying its behavior flowing through a continuous flow VAD it is possible to model it as a Newtonian fluid of viscosity $4 \cdot 10^{-3}$ Pa·s for a hematocrit of 45% [16, 17].

In the assistance of systemic circulation with a VAD, the pump must be able to fulfill the following physiological requirements: provide a mean pressure of 100 mmHg (for the systemic circulation, with a minimum value at 80 mmHg and a maximum value at 120 mmHg) and a flow rate of 5 L/min [4].

2.4 CFD simulation

The adopted computer simulation study examined the behavior of the flow in the devices under steady-state conditions. Thus, the Multiple Reference Frame model was employed, where the geometry inside the model, i.e., the space occupied by fluid, was divided into a moving region (encompassing the impeller) and a static region (containing the inlet and outlet ducts). Figure 2 schematically illustrates how these regions were obtained.

The mesh is composed of tetrahedral elements, where a constant rotation speed was assigned to the moving region of the mesh. Table 1 shows the element sizes as well as the mesh discretization for each model.
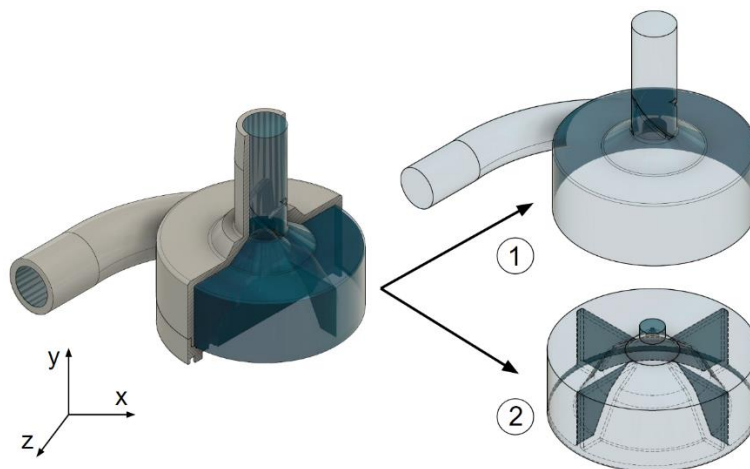

Figure 2: Schematization of how the static (1) and moving (or impeller - 2) regions were obtained. The coordinate system shown is the same used in all CFD simulations. The VAD-I1 model illustrates the example.

Table 1: Element size and mesh discretization for each model.

Model	Element Size [m]	Number of Elements
VAD-I1	$2.5 \cdot 10^{-4}$	7,561,146
VAD-DD1	$2.5 \cdot 10^{-4}$	3,768,588
VAD-R1/D1	$2.5 \cdot 10^{-4}$	6,232,425

For turbulence modeling, the viscous k-ω SST model was adopted. The k-ω SST model combines the treatment of flow close to the geometries' walls of the standard k-ω model with the treatment of flow away from the walls of the standard k-ε model [18]. The k-ω SST approach also gives more accurate results in estimating the pressure provided by the device [19].

Two sets of boundary conditions were adopted: a pressure boundary condition and a velocity boundary condition. Simulations with pressure boundary conditions were adopted to study the velocity contours, while velocity boundary conditions were adopted to obtain the pressure contours [18].

For the pressure boundary condition, a zero gauge pressure was applied to the inlet duct and a pressure of 25 mmHg to the outlet duct, in order to replicate the experimental conditions of the bench tests. As for the velocity boundary condition, the velocity applied to the inlet duct was defined based on the desired flow rate and duct diameter, while outflow condition was adopted for the outlet duct. The boundary condition adopted for the device walls was no-slip wall.

The coupling method adopted was SIMPLEC and the adopted gradient discretization was Green-Gauss node based. The solution initialization used the hybrid method, where the simulations were set up for 10,000 iterations.

2.4.1 Blood modeling and hemolysis estimation

The damage inflicted on RBCs was estimated using the model proposed by Giersiepen *et al.* [10] (equation 1). In it, the evaluation of pump-induced hemolysis through CFD simulations is done by relating the scalar shear stress τ (in Pa) to the exposure time t (in seconds) of the RBC to such stresses, obtaining the ratio between free hemoglobin in the blood and total hemoglobin in a sample [10, 16]:

$$\frac{\Delta H_b}{H_b}(\%) = 3{,}62 \cdot 10^{-5} \cdot \tau^{2{,}416} \cdot t^{0{,}785}$$

(1)

The scalar shear stress associated with the flow, described in Cartesian coordinates, is obtained by [14, 20, 21]:

$$\tau = \left[\frac{1}{6}\left[(\tau_x - \tau_y)^2 + (\tau_x - \tau_z)^2 + (\tau_y - \tau_z)^2\right] + \left(\tau_{xy}^2 + \tau_{yz}^2 + \tau_{zx}^2\right)\right]^{\frac{1}{2}}$$

(2)

Where the terms τ_x, τ_y, τ_z, τ_{xy}, τ_{yz}, and τ_{zx} are defined by:

$$\tau_x = -2\mu\frac{\partial v_x}{\partial x} \quad \tau_{xy} = -\mu\left(\frac{\partial v_x}{\partial y} + \frac{\partial v_y}{\partial x}\right)$$

$$\tau_y = -2\mu\frac{\partial v_y}{\partial y} \quad \tau_{yz} = -\mu\left(\frac{\partial v_y}{\partial z} + \frac{\partial v_z}{\partial y}\right)$$

$$\tau_z = -2\mu\frac{\partial v_z}{\partial z} \quad \tau_{zx} = -\mu\left(\frac{\partial v_z}{\partial x} + \frac{\partial v_x}{\partial z}\right)$$

With μ being the blood viscosity and $\partial v_u/\partial u$ being the strain rate.

The damage suffered by the RBCs (*D* in equation 3) is accumulated along their path inside the device [16, 20]. For a given exposure time discretization, the accumulated damage on a given trajectory is obtained by [20]:

$$D_i = D_{i-1} + (1 - D_{i-1})\frac{\Delta H_b}{H_b}$$

(3)

Where the $\Delta H_b/H_b$ function is expressed as a ratio. RBC destruction occurs for $D_i = 1$.

The mean damage for n distinct trajectories defines the RBC damage index [20]:

$$R_h = \frac{1}{n}\sum_{j=1}^{n} D_j$$

(4)

The approach for estimating the damage index on platelets, R_t, is analogous, where the model proposed by Giersiepen *et al.* [10] relates the release of the cytoplasmic enzyme lactate dehydrogenase (LDH) into plasma to the scalar shear stress and exposure time:

$$\frac{\Delta LDH}{LDH}(\%) = 3{,}31 \cdot 10^{-6} \cdot \tau^{3,075} \cdot t^{0,77}$$

(5)

For the model developed, the equations 1 and 5 are non-zero if a certain shear stress threshold is exceeded. Stresses above 150 Pa cause deformations that alter the functions of the RBCs, and for stresses above 300 Pa there is rupture of the cell membrane [15]. Whereas platelet activation occurs at stresses above 50 Pa [21]. Figure 3 schematizes the application of the thresholds.
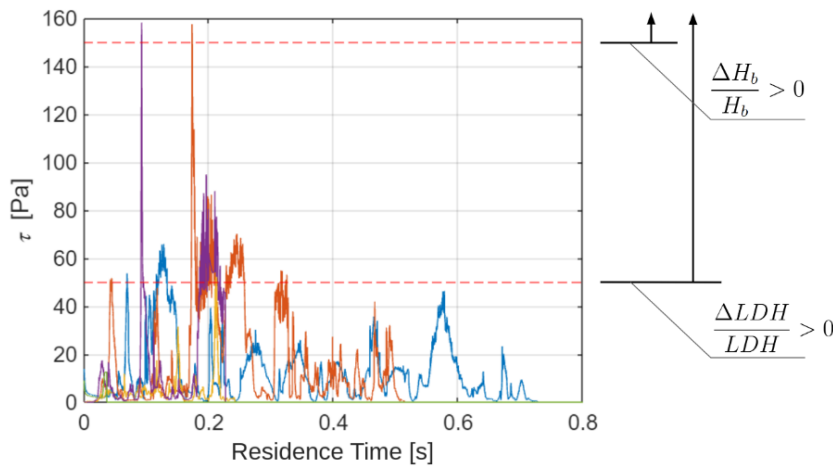

Figure 3: Schematization of the calculation of equations 1 and 5 from the scalar shear stress thresholds. The ratios are non-zero only when the thresholds associated with each cell type are exceeded.

The numerical modeling of blood considering the presence of RBCs and platelets adopted the Lagrangean approach with the inclusion of a discrete phase (Discrete Phase Model), which acts as a sample for determining the damage indices R_h and R_t [18, 21, 22]. The discrete phase is composed of spherical particles 8 μm in diameter (a simplification of the geometry of RBCs and platelets) configured to interact with the surrounding fluid. The effects of velocity fluctuation on the particles due to turbulence were estimated by stochastic tracking [22].
The boundary conditions adopted for this group of simulations were the same as those described for obtaining the pressure contours. The interaction of the particles with the walls was reflective. The tracking data was obtained from a sample of 100 particles.

2.5 Bench testing

A schematic of the test bench is shown in figure 4. The test fluid was stored in two height-adjustable tanks (T1 and T2) and was pumped by the VAD from T1 to T2. The VAD is powered by a DC motor attached to a barrel with neodymium magnets (AM element in figure 5), so the coupling between the device's impeller and the DC motor is magnetic. An encoder associated with the motor shaft is responsible for measuring the rotational speed. The level of the tanks is monitored by sensors whose state variation is responsible for triggering an external pump that takes the fluid from tank T2 to tank T1. The elements P, SF and V in figure 4 are a pressure sensor, a flow sensor and a valve, respectively. The pressure sensor is a piezometer that measures the static pressure near the output duct of the VAD. The valve allows the control of its aperture level via software.

Water was adopted as the test fluid when obtaining the characteristic curves on the test bench. The T1 tank was positioned at approximately the same height as the VAD inlet duct, while the T2 tank was at an initial height that provided a pressure of approximately 25 mmHg (minimum height allowed by the experimental apparatus).
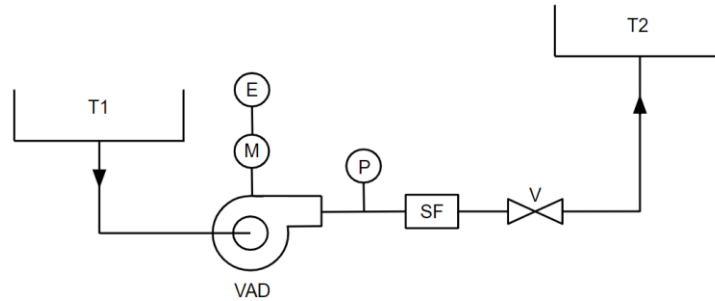

Figure 4: Schematic of the test bench highlighting its main components: T1 and T2 are the test fluid storage tanks, M refers to the DC motor coupled to the VAD, E is the encoder, P the pressure sensor, SF the flow sensor, and V the valve with adjustable opening. The flow direction is indicated by arrows. The level sensors, the magnetic coupling of the VAD and the external pump are omitted.
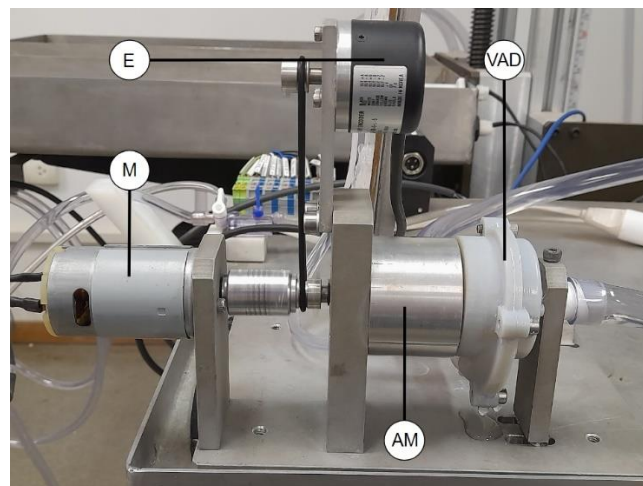

Figure 5: Detail of the pump assembly during a test of the VAD-R1/D1 device. Highlighted are the DC motor, the encoder, the magnetic coupling (AM), and the VAD. The coupling between the encoder and the motor is done by a belt.

The rotational speed curves are obtained by varying the rotational speed of the VAD motor and taking flow rate measurements. In turn, the pressure curves are plotted from the variation of height of the T2 tank maintaining a fixed rotational speed of the VAD's motor, monitoring the water column (taken as the pressure in the device's outlet duct) and the flow rate.

3. RESULTS

3.1 CFD simulations

Analyses of the velocity and pressure contours were made from planes sectioning the devices, obtaining cross-sections of the inlet and outlet ducts. For this set of simulations, water as the fluid and a rotation of 2,000 rpm (positive towards the y axis, following the coordinate system illustrated in figure 2) were adopted. From this first analysis, the presence of critical zones was identified, which were then examined using velocity vectors.

Possible recirculation regions are identified through the contours by the steep drop in velocity. Figure 6 exemplifies a recirculation region near the base of the outlet duct of the VAD-I1 model. The vortex behavior is then evidenced by velocity vectors (figure 7). The formation of such

critical zones in the outlet duct are common to all models (figure 8). Recirculation is also seen at the base of the inlet duct on the VAD-I1 and VAD-DD1 models.
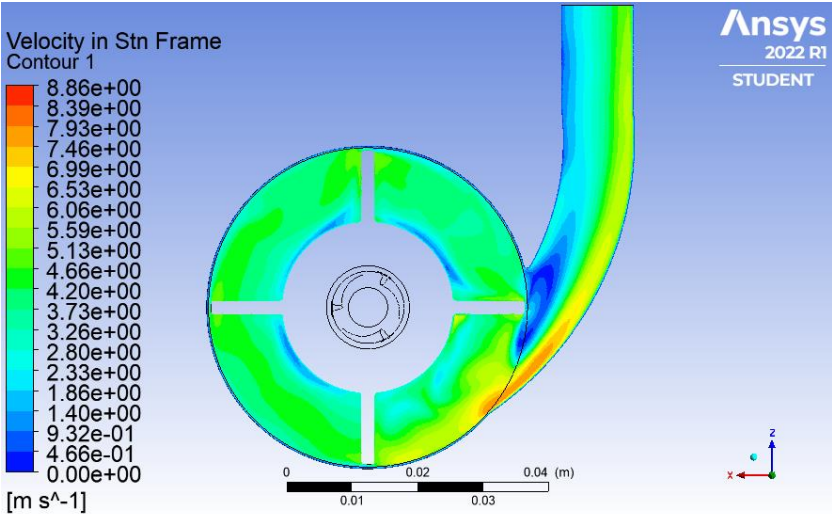

Figure 6: Velocity contour for model VAD-I1. The recirculation region is indicated by the steep drop in velocity at the base of the outlet duct.
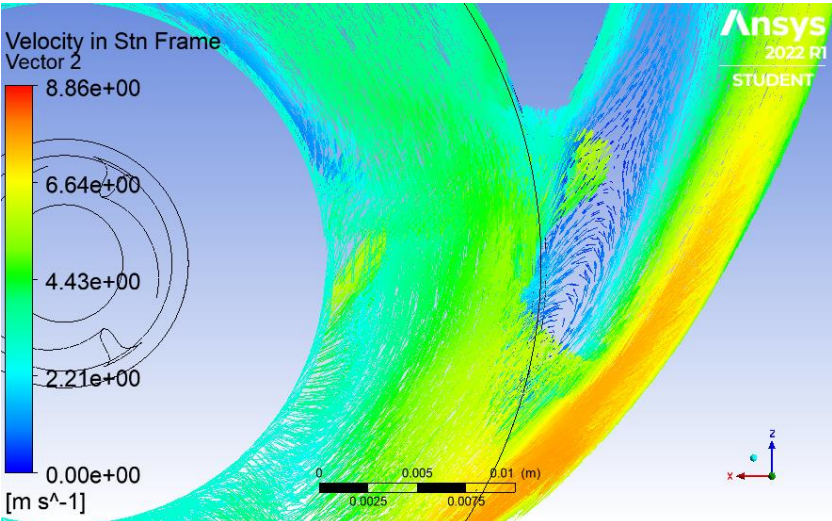

Figure 7: Distribution of velocity vectors in a detail of the base of the outlet duct. Note the formation of vortices.
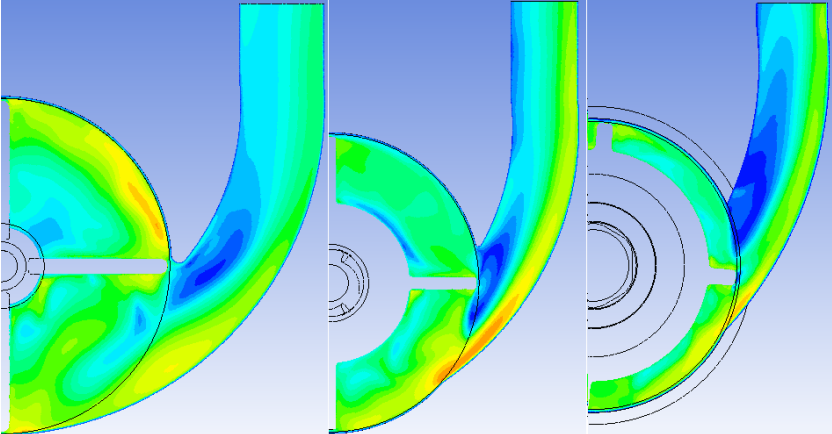

Figure 8: Velocity contours in the region of the outlet duct of studied models. From left to right, the models VAD-R1/D1, VAD-I1 and VAD-DD1 are illustrated.

The particular structures of each model were also studied. The velocity vectors in a plane tangent to the bottom edge of the thread of model VAD-I1 are shown in figure 9. Although the thread fulfills its role in directing the flow, the generation of vortices behind the thread may contribute to thrombus formation. The contact bearing support associated with the inlet duct of the VAD-R1/D1 model has a region of flow stagnation at its junction with the duct (figure 10).
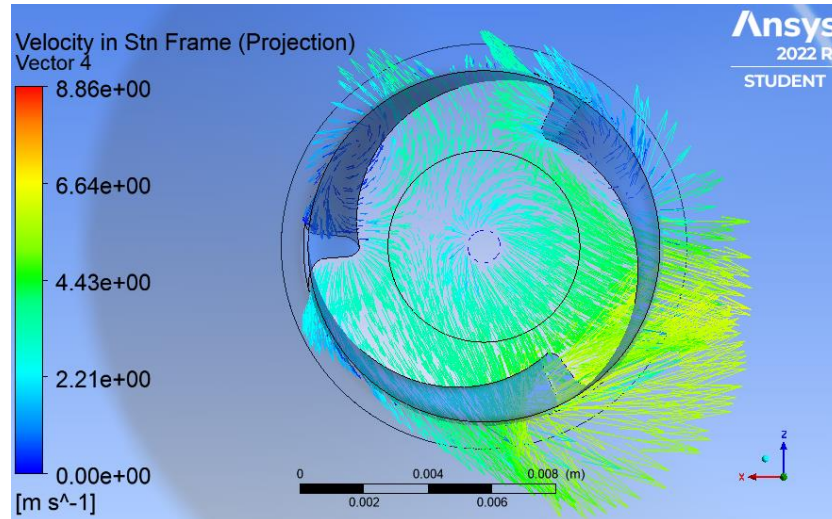

Figure 9: Velocity vectors projected onto a plane located at the end of the inlet duct thread.
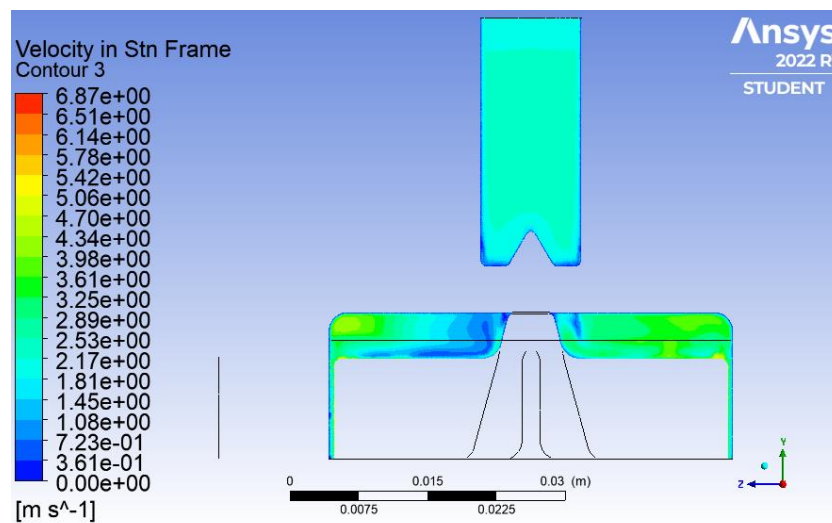

Figure 10: Velocity contour in a plane sectioning the inlet duct and the contact bearing support of model VAD-R1/D1.

Figure 11 presents the characteristic curves obtained through CFD simulations for each model. The rotational speed curves (figure 11a) were obtained by varying, in each simulation, the rotational speed assigned to the impeller. The pressure curves (figure 11b) were obtained by varying the fluid inlet velocity to a constant rotational speed. The pressure values shown are total pressure.

Table 2 gathers the minimum expected rotational speeds for the devices given the adopted simulation conditions and the parameter $\Delta P/\Delta Q$, which represents the pressure variation over the same flow rate range (from 4 L/min to 6 L/min). A low pressure variation for a given flow variation is characteristic of centrifugal pumps. This characteristic has operational advantages, such as avoiding ventricular wall suction episodes and better preservation of the natural pulsatility of blood flow [4, 23]. Data from the literature are also presented for comparison.

An estimation of the hemolysis caused by the devices applying the blood model developed is presented by table 3. This set of simulations adopts the rotational speed that satisfies the physiological requirements (pressure of 100 mmHg for a flow rate of 5 L/min), ω_f, determined in simulations with water.
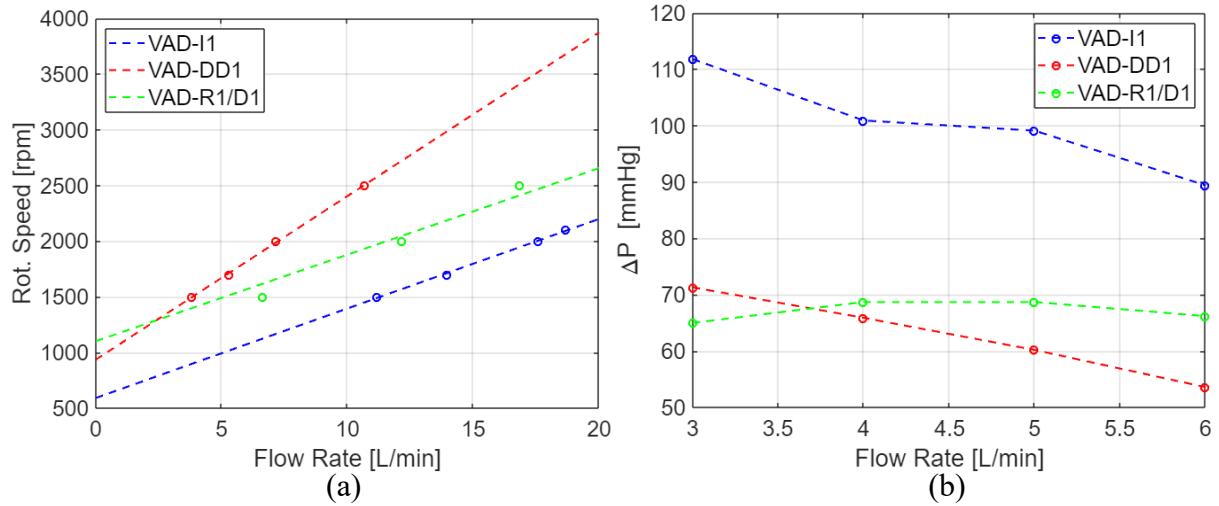

Figure 11: Characteristic curves of each model: (a) rotational speed curve; and (b) pressure curves for a rotational speed of 2,000 rpm.

Table 2: Parameters obtained by simulation of the studied devices and comparison with literature data. The ratio $\Delta P/\Delta Q$ (given in mmHg·min/L) was obtained for the same flow rate range (from 4 L/min to 6 L/min). Moazami *et al.* [23] presents the curve for the commercial device DuraHeart (Terumo Heart Inc.), while Bock *et al.* [24] presents the curve for the device under development by the partnership of the Dante Pazzanese Institute of Cardiology and Baylor College of Medicine.

Model	Min. Speed [rpm]	$\dfrac{\Delta P}{\Delta Q}$	$\dfrac{\Delta P}{\Delta Q}$ [23]	$\dfrac{\Delta P}{\Delta Q}$ [24]
VAD-I1	591.6	5.8		
VAD-DD1	936.2	6.2	9.4	14.1
VAD-R1/D1	1102.0	1.3		

Table 3: Results of simulations estimating hemolysis. In addition to the damage indices and the average residence time ($\overline{\Delta t}$), the rotational speed at which the physiological requirements were met (ω_f) is also presented.

Model	ω_f [rpm]	R_h [%]	R_t [%]	$\overline{\Delta t}$ [s]
VAD-I1	2000	2.0	69.1	0.636 ± 0.423
VAD-DD1	2500	7.4	43.9	0.152 ± 0.122
VAD-R1/D1	2300	0.0	49.3	0.349 ± 0.248

The shear stress distribution associated with the device walls are illustrated by figures 12 and 13 (the results from the VAD-DD1 model are used as an example). Stresses ≥ 300 Pa get the maximum coloring of the scale. The outlet duct opening and the extremities of the impeller blades were common critical areas for all devices. The support of the contact bearing on the inlet duct of the VAD-R1/D1 model was also studied, where the highest stresses experienced were about 200 Pa, occurring in small regions along the sides of the blood passage opening.
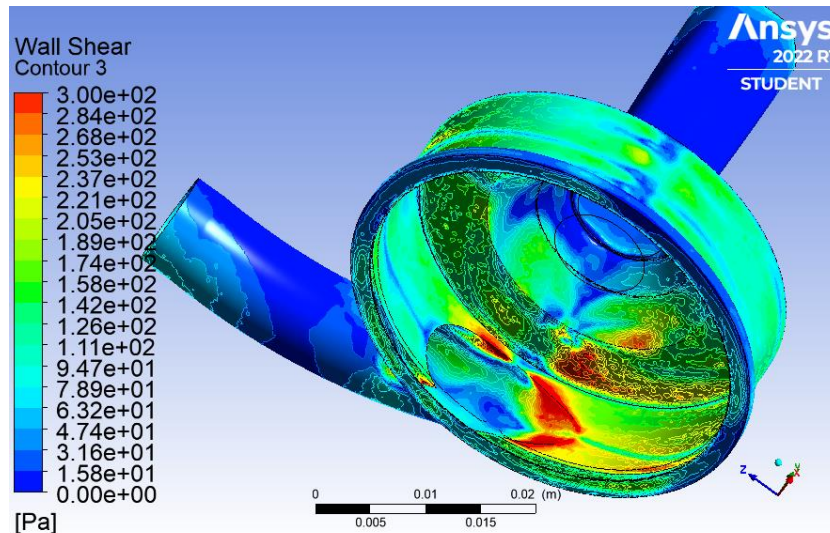
Figure 12: Shear stress distribution associated with the walls of the device housing. Noteworthy is the presence of critical zones around the outlet duct opening. The VAD-DD1 model is used in the illustrated example.
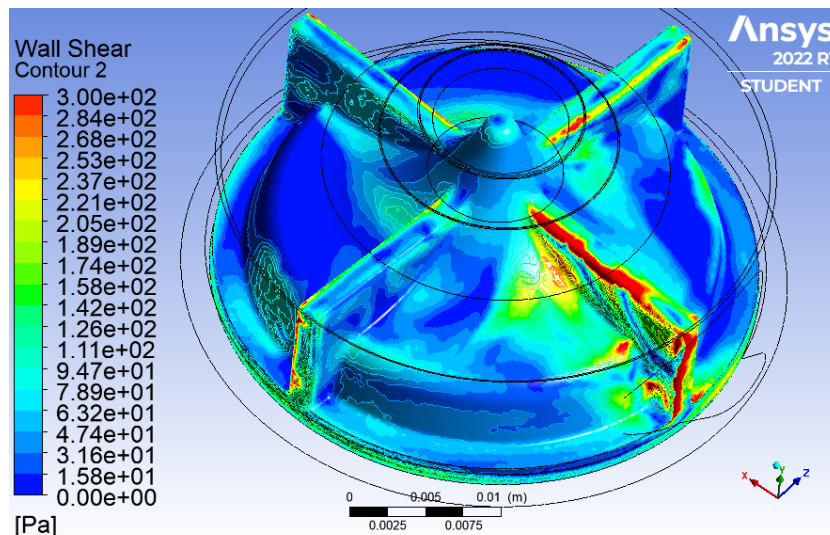

Figure 13: Shear stress distribution associated with the walls of the impeller. The main critical zones appear at the blade extremities. The VAD-DD1 model illustrates the example.

3.2 Bench testing

The bench tests were performed with the prototype of the VAD-R1/D1 model.

In the plot of the rotational speed curve (figure 14a), two heights were adopted for tank T2: one equivalent to a pressure of approximately 25 mmHg and the other equivalent to approximately 65 mmHg. For the experimental settings adopted, the minimum rotational speeds of the device are approximately 750 rpm and 1,600 rpm for the heights of 25 mmHg and 65 mmHg respectively.

Figure 14b illustrates the variation of pressure as a function of flow for three fixed rotational speeds. A subtle pressure drop is observed as the flow rate increases, which is characteristic of centrifugal pumps. For a rotation of 2,000 rpm and a variation of approximately 2 L/min, a pressure drop of approximately 12 mmHg occurred.
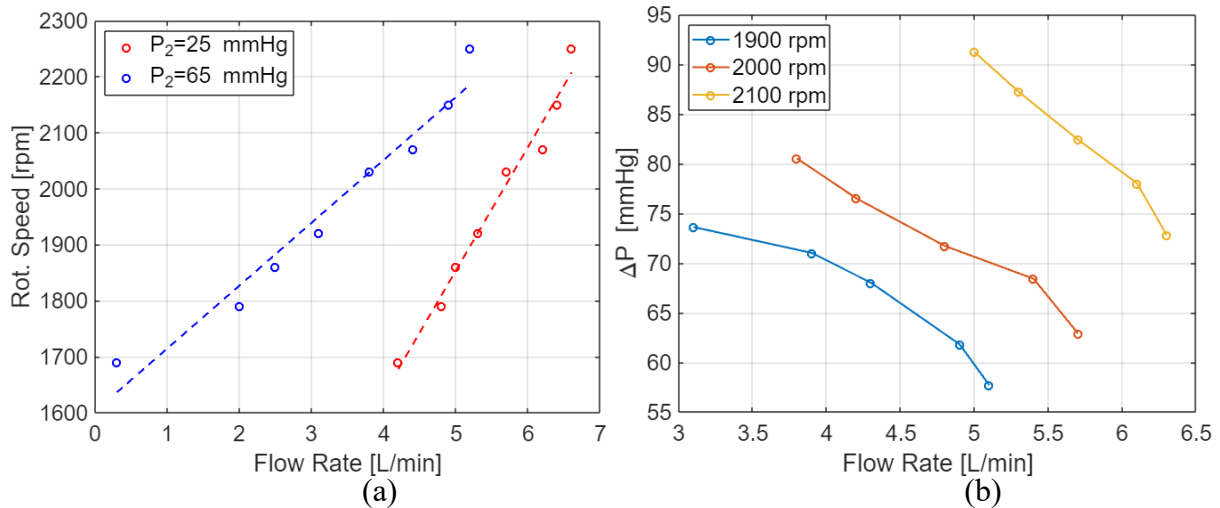
Figure 14: Characteristic curves of each model: (a) rotational speed curve for two heights of tank T2; and (b) pressure versus flow curves for a set of rotational speeds.

4. DISCUSSION

From the analysis of the velocity contours, it was possible to observe the influence of the device geometry on the location and magnitude of critical zones, in particular, recirculation regions (figure 8). When the outlet duct opening follows the curvature of the device housing (as in VAD-R1/D1), the magnitude of the critical zone is reduced and it forms further downstream of the duct. In contrast, when the outlet duct opening appears abruptly in the housing (as in VAD-DD1), the critical zone becomes more severe and is formed further upstream. The effect seems to be opposite for the inlet duct: a smoother transition between the inlet duct and the device housing (as in the VAD-I1 and VAD-DD1 models) favors the formation of recirculation regions, while a steeper transition (as in VAD-R1/D1) reduces their appearance.

From the characteristic curves (figure 11), it can be concluded that the VAD-I1 model showed the best energy performance, achieving higher flow rates for lower rotational speeds and comparatively higher pressures for a given rotation. While the physiological requirements were met for the VAD-I1 device at a rotation of 2,000 rpm, the same occurred for the VAD-DD1 device at a rotation of 2,500 rpm and for the VAD-R1/D1 at 2,300 rpm. Considering the parameter $\Delta P/\Delta Q$, the VAD-R1/D1 model presented the best performance.

Based on the analysis of the velocity contours, a qualitative evaluation of the thrombogenicity of the devices is done: the formation of recirculation regions in the outlet duct was common to all the models studied, this being an eventual redesign point; regarding the inlet duct, both the VAD-I1 and the VAD-DD1 showed recirculation in regions close to the walls of the base of the duct, which may favor thrombus formation. Elements such as the thread and bearing support present in the VAD-I1 and VAD-R1/D1 devices respectively, also showed critical zones that may contribute to thrombogenicity.

The geometry of the device impacts the shear stress distribution associated with the walls. The abrupt transition from the VAD housing to the output duct generates larger critical zones. Despite the smoother transition of the VAD-R1/D1, the VAD-I1 device had the smallest regions with high shear stresses around the outlet duct opening. Such phenomenon may be linked to the geometry of the impeller or the distance between the impeller blades and the housing (0.8 mm for VAD-I1 and 0.5 mm for the others).

Considering the R_h index, the VAD-R1/D1 presented the best performance, where no damage was identified for the method used. As for the R_t index, the best performance was observed for the VAD-DD1 device, also exhibiting the shortest average residence time.

Although Giersiepen's *et al*. method overestimates the damage indices [11, 25], the approach adopted in this paper was conservative, so actual indices are probably higher than the obtained data. The 1 and 5 equations were applied only when the shear stress thresholds were surpassed, not considering how long the particles remained under stresses below them. Thus, any potential damage caused by low shear stresses acting over a prolonged exposure time was ignored. Still, according to Wu *et al*. [16], the R_h index should not be higher than 4%.

One can observe that the best performance for each damage index occurred for different devices. This is due to the fact that more particles experience shear stresses above 50 Pa for the VAD-R1/D1 device, although none exceed 150 Pa. In contrast, for VAD-DD1, more particles experience stresses above 150 Pa, although most of the sample does not reach the 50 Pa threshold.

The results obtained in CFD simulation and those obtained on the test bench were compared (figure 15). From the rotational speed curves, it is noticeable that the performance of the simulated model is better than that of the prototype (higher flow rates for lower rotational speeds). The methodologies adopted in obtaining these curves were, therefore, compatible, requiring efficiency or correction factors to better fit the simulation model. The comparison between the pressure curves resulted in an incongruent behavior. Such difference may reside in the incompatibility of the methodologies used: in the CFD simulation the flow rate was described as a function of the fluid inlet velocity, i.e., the variable is directly controlled; in the bench tests the flow rate was changed by applying different pressures on the outlet duct (i.e., changing the height of the T2 tank), thus the control of the variable is indirect. However, for the two rotational speeds adopted, the simulation model and the bench tests showed close pressures for flow rates around 5 L/min (for 1900 rpm the maximum error between 4.5 L/min and 5 L/min is 10%, and for 2000 rpm between 4.5 L/min and 5.5 L/min is 7%).
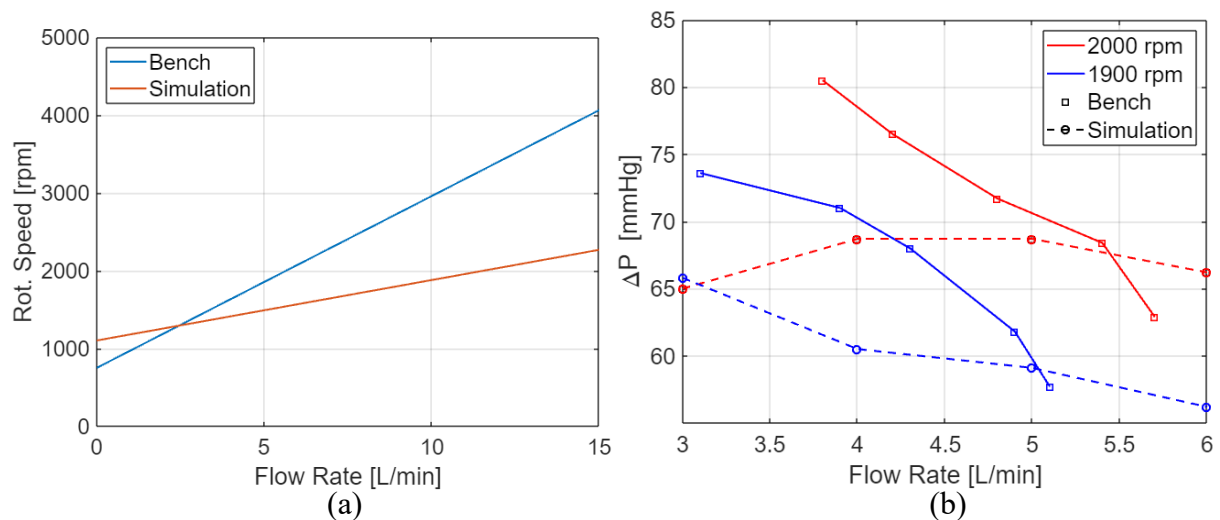

Figure 15: Results obtained on the test bench and in CFD simulation are compared. The rotational speed curves are presented in (a). The pressure curves for two rotational speed sets are shown in (b).

5. CONCLUSION

CVDs have an important participation in the number of deaths in Brazil. Although heart transplant, when applicable, makes it possible to increase the life expectancy of patients, the national hospital structure and the number of donors offer severe limitations to this approach. Thus, VADs present themselves as an alternative, enabling the return, to some degree, of the patient's daily activities, ensuring a better quality of life. The democratization of this type of therapy, therefore, is a humanitarian issue.

CFD simulations are an essential part of the VAD development process. They act as a tool to assist the device optimization prior to more costly design phases such as prototype testing and *in vitro* trials.

The methodology presented for the hydrodynamic simulations was able to point out regions of recirculation in the models, including the influence of geometry on the magnitude and behavior of these critical zones. Based on these results, it was possible to discuss, qualitatively, the thrombogenicity of the devices. The methods used, also made it possible to raise the characteristic curves, indicating relevant parameters of each model, such as the minimum operating speed, the $\Delta P/\Delta Q$ and the rotational speed that meets the physiological requirements. The blood damage estimation model and blood modeling provided a preliminary assessment of hemolysis and platelet activation, although the results were conservative. These models, along with the shear stress contours on the device walls, prompt a prior discussion on the necessity for optimization of elements associated with hemolysis, such as the geometry of the impeller.

The bench tests acted as an evaluator of the methods used. Corrective factors or adjustments to the adopted methodology are needed. Although a discrepancy was observed with respect to the pressure curves obtained in simulation and on the test bench, the errors, in general, were below 20%.

Analyzing the results obtained altogether, the VAD-I1 and VAD-R1/D1 models showed the best performances. While the VAD-I1 exhibited the best energy performance and smaller critical zones for shear stresses in its walls, the VAD-R1/D1 showed recirculation regions of smaller magnitude, the smallest $\Delta P/\Delta Q$ parameter, and the lowest R_h index.

6. ACKNOWLEDGMENT

REFERENCES

[1] C. W. Tsao *et al.*, "Heart Disease and Stroke Statistics—2022 Update: A Report From the American Heart Association," *Circulation*, vol. 145, no. 8, Feb. 2022, doi: 10.1161/CIR.0000000000001052.

[2] Sociedade Brasileira de Cardiologia, "CARDIÔMETRO Mortes por Doenças Cardiovasculares no Brasil," *CARDIÔMETRO*. http://www.cardiometro.com.br (accessed Apr. 12, 2021).

[3] M. Hosseinipour, R. Gupta, M. Bonnell, and M. Elahinia, "Rotary mechanical circulatory support systems," *Journal of Rehabilitation and Assistive Technologies Engineering*, vol. 4, p. 205566831772599, Jan. 2017, doi: 10.1177/2055668317725994.

[4] T. Yamane, *Mechanism of Artificial Heart*. Tokyo: Springer Japan, 2016. doi: 10.1007/978-4-431-55831-6.

[5] S. Agarwal and K. M. High, "Newer-generation ventricular assist devices," *Best Practice & Research Clinical Anaesthesiology*, vol. 26, no. 2, pp. 117–130, Jun. 2012, doi: 10.1016/j.bpa.2012.01.003.

[6] L. S. da S. Soares, E. S. de Brito, L. Magedanz, F. A. França, W. N. de Araújo, and D. Galato, "Transplantes de órgãos sólidos no Brasil: estudo descritivo sobre desigualdades na distribuição e acesso no território brasileiro, 2001-2017*," *Epidemiologia e Serviços de Saúde*, vol. 29, no. 1, Apr. 2020, doi: 10.5123/S1679-49742020000100014.

[7] L. F. P. Moreira and A. Benício, "Assistência circulatória mecânica: uma grande lacuna na cirurgia cardíaca brasileira," *Rev Bras Cir Cardiovasc*, vol. 25, no. 4, p. X–XII, Dec. 2010, doi: 10.1590/S0102-76382010000400005.

[8]   Mariana Maria Aparecida Pinto Hernandes, "Análise do Escoamento em um Dispositivo de Assistência Ventricular," Mestrado, Instituto Federal de Educação, Ciência e Tecnologia de São Paulo, São Paulo, Brasil, 2018.

[9]   P. Shah, U. S. Tantry, K. P. Bliden, and P. A. Gurbel, "Bleeding and thrombosis associated with ventricular assist device therapy," *The Journal of Heart and Lung Transplantation*, vol. 36, no. 11, pp. 1164–1173, Nov. 2017, doi: 10.1016/j.healun.2017.05.008.

[10]   M. Giersiepen, L. J. Wurzinger, R. Opitz, and H. Reul, "Estimation of Shear Stress-related Blood Damage in Heart Valve Prostheses - in Vitro Comparison of 25 Aortic Valves," *The International Journal of Artificial Organs*, vol. 13, no. 5, pp. 300–306, May 1990, doi: 10.1177/039139889001300507.

[11]   H. Schima, G. Wieselthaler, I. Schwendenwein, U. Losert, and E. Wolner, "A Review and Assessment of Investigative Methods for Mechanically Induced Blood Trauma: Special Aspects in Rotary Blood Pumps," in *Heart Replacement*, T. Akutsu and H. Koyanagi, Eds., Tokyo: Springer Japan, 1998, pp. 361–369. doi: 10.1007/978-4-431-65921-1_53.

[12]   W.-C. Chiu *et al.*, "Thromboresistance Comparison of the HeartMate II Ventricular Assist Device With the Device Thrombogenicity Emulation-Optimized HeartAssist 5 VAD," *Journal of Biomechanical Engineering*, vol. 136, no. 2, p. 021014, Feb. 2014, doi: 10.1115/1.4026254.

[13]   D. Bluestein, S. Einav, and M. J. Slepian, "Device thrombogenicity emulation: A novel methodology for optimizing the thromboresistance of cardiovascular devices," *Journal of Biomechanics*, vol. 46, no. 2, pp. 338–344, Jan. 2013, doi: 10.1016/j.jbiomech.2012.11.033.

[14]   M. Behbahani *et al.*, "A review of computational fluid dynamics analysis of blood pumps," *Eur. J. Appl. Math*, vol. 20, no. 4, pp. 363–397, Aug. 2009, doi: 10.1017/S0956792509007839.

[15]   C. G. Nevaril, J. D. Hellums, C. P. Alfrey, and E. C. Lynch, "Physical effects in red blood cell trauma," *AIChE J.*, vol. 15, no. 5, pp. 707–711, Sep. 1969, doi: 10.1002/aic.690150514.

[16]   H. Wu, "Structural Design and Numerical Simulation of an Implantable Axial Blood Pump," *OAJBS*, vol. 1, no. 3, Nov. 2019, doi: 10.38125/OAJBS.000121.

[17]   M. Kutz, *Biomedical Engineering and Design Handbook, Volumes I and II (2nd Edition)*. New York, USA: McGraw-Hill Professional Publishing, 2010. Accessed: Jun. 18, 2021. [Online]. Available: http://public.ebookcentral.proquest.com/choice/publicfullrecord.aspx?p=4657812

[18]   G. B. Lopes Junior, "Metodologia para análise computacional de escoamento sanguíneo em dispositivos de assistência ventricular," Doutorado em Térmica e Fluidos, Universidade de São Paulo, São Carlos, 2016. doi: 10.11606/T.18.2016.tde-21072016-092253.

[19]   K. H. Fraser, T. Zhang, M. E. Taskin, B. P. Griffith, and Z. J. Wu, "A Quantitative Comparison of Mechanical Blood Damage Parameters in Rotary Ventricular Assist Devices: Shear Stress, Exposure Time and Hemolysis Index," *Journal of Biomechanical Engineering*, vol. 134, no. 8, p. 081002, Aug. 2012, doi: 10.1115/1.4007092.

[20]   A. Mitoh *et al.*, "Shear stress evaluation on blood cells using computational fluid dynamics," *BME*, vol. 31, no. 3, pp. 169–178, Jul. 2020, doi: 10.3233/BME-201088.

[21]   A. Romanova and D. Telyshev, "Computational fluid dynamics simulation of hemolysis at different levels of circulatory support in the left ventricular assist device Sputnik," *J. Phys.: Conf. Ser.*, vol. 2091, no. 1, p. 012021, Nov. 2021, doi: 10.1088/1742-6596/2091/1/012021.

[22] *ANSYS Fluent User's Guide*, Release 15.0. ANSYS Inc., 2013.

[23] N. Moazami *et al.*, "Axial and centrifugal continuous-flow rotary pumps: A translation from pump mechanics to clinical practice," *The Journal of Heart and Lung Transplantation*, vol. 32, no. 1, pp. 1–11, Jan. 2013, doi: 10.1016/j.healun.2012.10.001.

[24] E. Bock *et al.*, "New Centrifugal Blood Pump With Dual Impeller and Double Pivot Bearing System: Wear Evaluation in Bearing System, Performance Tests, and Preliminary Hemolysis Tests," *Artificial Organs*, vol. 32, no. 4, pp. 329–333, Apr. 2008, doi: 10.1111/j.1525-1594.2008.00550.x.

[25] T. Yano *et al.*, "An Estimation Method of Hemolysis within an Axial Flow Blood Pump by Computational Fluid Dynamics Analysis," *Artificial Organs*, vol. 27, no. 10, pp. 920–925, Oct. 2003, doi: 10.1046/j.1525-1594.2003.00034.x.

CONTACTS

Victor Figueiredo Soares   email: victor.figueiredo.soares@usp.br

Prof. Dr. R. Lima Stoeterau   email: rodrigo.stoeterau@usp.br